Journal of
Materials Chemistry C

REVIEW

View Article Online
View Journal

Cite this: DOI: 10.1039/c5tc01670c

Strategies for engineering phonon transport in thermoelectrics

Woochul Kim

Received 7th June 2015,
Accepted 21st July 2015

DOI: 10.1039/c5tc01670c

www.rsc.org/MaterialsC

In this review, we discuss some of the representative strategies of phonon engineering by categorizing them into the methods affecting each component of phonon thermal conductivity, *i.e.*, specific heat, phonon group velocity, and mean free path. In terms of specific heat, a large unit cell is beneficial in that it can minimize the fraction of thermal energy that can be transported since most of the energy is stored in the optical branches. In an artificial structure such as the superlattice, phonon bandgaps can be created through constructive interference by Bragg reflection, which reduces phonon group velocity. We further categorize the mean free path, *i.e.*, scattering processes, into grain boundary scattering, impurity scattering, and phonon–phonon scattering. Rough-surfaced grains, nano-sized grains, and coated grains are discussed for enhancement of the grain boundary scattering. Alloy atoms, vacancies, nanoparticles, and nano-sized holes are treated as impurities, which limit the phonon mean free path. Lone pair electrons and acoustical-to-optical scattering are suggested for manipulating phonon–phonon scattering. We also briefly mention the limitation and temperature range in which the Wiedemann–Franz law is valid in order to achieve a better estimation of electronic thermal conductivity. This paper provides an organized view of phonon engineering so that this concept can be implemented synergistically with power factor enhancement approaches for design of thermoelectric materials.

1. Introduction

A thermoelectric (TE) device is a solid-state device that converts heat directly into electricity based on the Seebeck effect and refrigerates objects by supplying electricity due to the Peltier effect.[1–4] Such a device can be used for both power generation and refrigeration. Among the numerous advantages of these devices, such as simplicity and smaller space requirements than other heat engines and compressor-based refrigerators, the reliability due to the lack of moving parts can be the most useful feature. For example, a TE device has been used in a space mission as a power generator, *i.e.*, a radioisotope thermoelectric generator (RTG), and has demonstrated long-term reliability.[4] Especially, the RTGs in Voyagers 1 and 2 have been operating unmaintained ever since they were launched in 1977.[5] However, the low conversion efficiency of the device hinders it from wide practical application. The conversion efficiency of the device is related to its material parameter of thermoelectric figure of merit, zT,

$$zT = \frac{S^2\sigma T}{k_{\text{total}}} = \frac{S^2\sigma T}{k_{\text{L}} + k_{\text{e}}} \quad (1)$$

where T is the absolute temperature, S is the Seebeck coefficient, σ is the electrical conductivity, and k_{total}, k_{L} and k_{e} are the total, phonon (lattice), and electronic thermal conductivities, respectively. It is not trivial to increase zT since those three parameters are interdependent; increasing one usually decreases the others.[3,4] Semiconductors are the ideal material for TE devices because they have higher zT values than insulators, metals, and semi-metals. Therefore, since the discovery of semiconductors,

School of Mechanical Engineering, Yonsei University, Seoul 120-749, Korea.
E-mail: woochul@yonsei.ac.kr

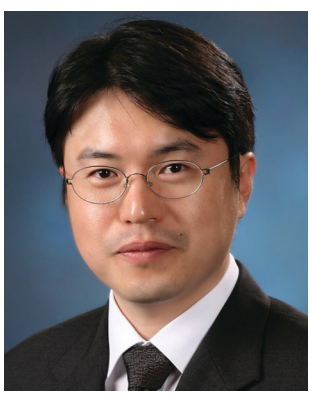

Woochul Kim

Prof. Woochul Kim received his PhD at U. C. Berkeley in 2005. Then, after one and a half years as a postdoctoral researcher, he has been working in Yonsei University as an assistant, associate professor since 2007. He is a consulting professor at LG Innotek and a principal investigator for the 'National Leading Research Laboratory' supported by the Korean government. He was the recipient of the Young Thermal Engineer Award by KSME (Korean Society of Mechanical Engineers) in 2013 and the Netzsch KSTP TPP award in 2015 by KSTP (Korean Society of Thermophysical Properties).

efforts have been made to increase their zT values, resulting in zT values greater than 2.0.[6–10]

In solids, thermal energy can be transported in two ways: through electrons and through lattice vibrations. In good electrical conductors like metals, electrons are the dominant heat carriers, whereas lattice vibrations are responsible for energy transport in many non-metals, such as semiconductors and dielectric solids. This work concentrates on thermal transport by lattice vibration in crystalline non-metals since most thermoelectric materials are semiconductors.

In this review, we focus on strategies for decreasing the phonon thermal conductivity in thermoelectric applications and categorize those strategies, which typically consist of combined effects of multiple strategies (see Fig. 1). For example, DiSalvo[11] and Slack[3] proposed that thermal conductivity can be lowered in compounds that have a low melting point, heavy elements, and a large unit cell. The low melting point is related to the low elastic modulus, which leads to low sound velocity, *i.e.*, low phonon group velocity. The heavy elements also reduce the sound velocity. The large unit cell decreases the fraction of energy transported through the acoustic modes, which is related to the specific heat.

The phonon thermal conductivity can be expressed using the following relationship, which is confirmed by kinetic theory[12] and the Boltzmann transport equation.[13,14]

$$k_{\mathrm{L}} = \frac{1}{3}\int C_{\mathrm{v}}(\omega)\cdot\nu(\omega)\cdot l(\omega)\mathrm{d}\omega \qquad (2)$$

where C_{v} is the specific heat, ν is the phonon group velocity, l is the phonon mean free path (or the scattering processes), and ω is the phonon frequency. Next, we investigate methods for reducing each individual parameter.

2. Engineering phonon thermal conductivity

a. Specific heat, C_{v}

The specific heat in eqn (2) is based on the partial derivative of the total energy of the phonons[12] with respect to temperature at

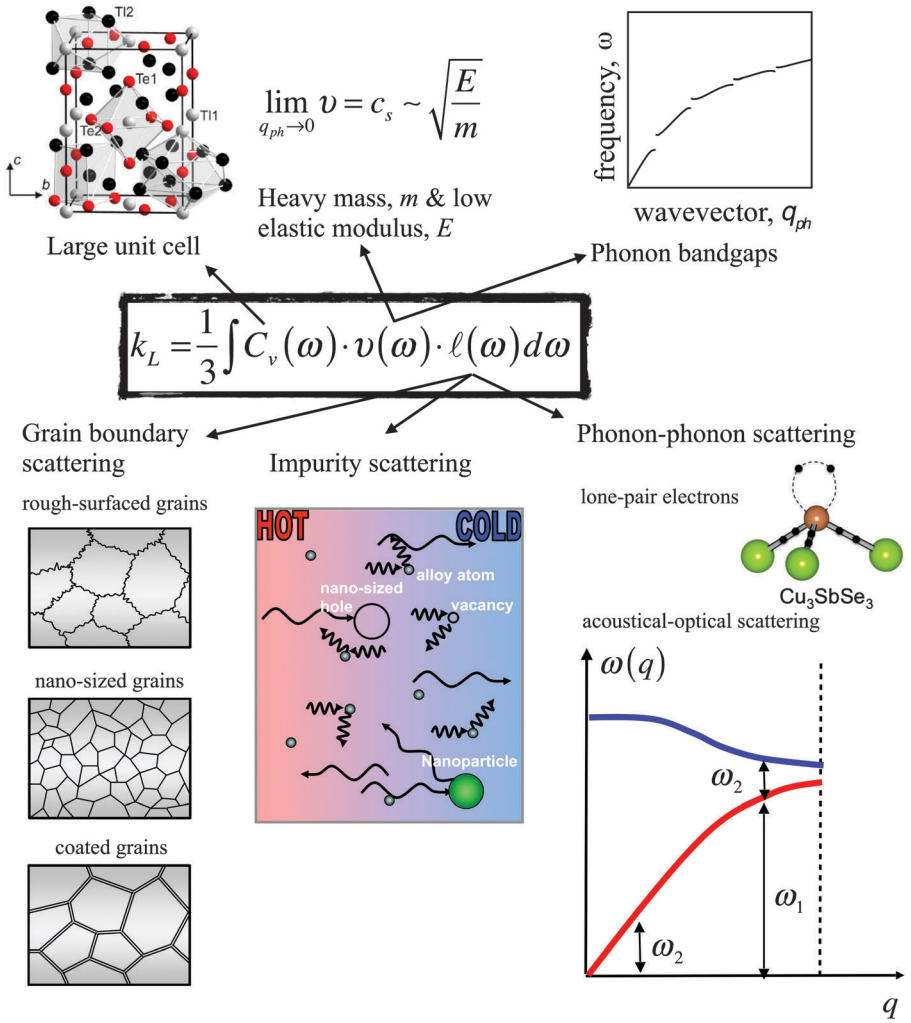

Fig. 1 Strategies of phonon engineering categorized into methods affecting each component of phonon thermal conductivity, *i.e.*, specific heat, phonon group velocity, and scattering processes. Some of the figures are from the literature.[71,80] Copyright © 2013, American Chemical Society, and Copyright © 2011 American Physical Society.

constant volume. Tuning the specific heat to eventually change the thermal conductivity is very difficult unless the size of the crystal is on the order of the atomic scale so that the lattice vibrations are confined and the dispersion relation is modified. Instead, we present the large unit cell approach, *i.e.*, search for a crystal with a large number of atoms in a unit cell, to control the specific heat. However, as a consequence of this effect, other parameters such as reduced phonon group velocity due to the flattening of the phonon dispersion relationship and enhanced inter-branch scattering owing to the creation of many optical branches. In a solid, energy can be absorbed by either acoustic or optical phonons. In a general case in which there are p atoms in a unit cell and G unit cells in the crystal, there will be $3pG$ normal modes and $3p$ branches. Three of the branches are acoustic and the rest are optical branches, *i.e.*, $3p - 3$, since the acoustic branches have three polarizations, one longitudinal and two transverse. The number of acoustic branches is always three despite the number of atoms in the unit cell. Considering that optical phonons do not contribute to heat conduction since their propagation speed is close to zero,[13] it is beneficial to have large p in a unit cell in order to achieve low thermal conductivity. When the crystal absorbs energy, only a fraction of the energy can be transported through the acoustic branches.

Fig. 2 shows the phonon dispersion curves of diamond-structured Ge, guest-free clathrate Ge_{46}, and guest-containing Sr_6Ge_{46}, respectively.[15] The Ge_{46} is supposed to have three acoustic branches and 135 optical branches, as shown in the figure. Also, since the maximum phonon frequency is limited to $\sim$10 THz, the ranges of acoustic phonon frequency decrease as the number of optical branches increases. Therefore, the phonon group velocity, *i.e.*, the slope of the acoustic branch, also decreases, which further reduces the thermal conductivity. In a similar example, Wölfing *et al.*[16] reported an extremely low phonon thermal conductivity of Tl_9BiTe_6 of 0.39 W m^{-1} K^{-1} at 300 K. The number of atoms in a unit cell of this material is as large as 32,[17] which indicates that there are three acoustic branches and 93 optical branches. Considering that there are two atoms in PbTe and five atoms in Bi_2Te_3, this number is quite high. However, in this kind of material, further reducing the thermal conductivity by incorporation of alloy atoms, *i.e.*, alloy scattering, is not trivial[18] because there are many atoms with different masses and force constants that result in scattering of high-frequency phonons. Introduction of additional atoms for alloy scattering is of no further use. Another example of a material in this category is $Sr_4Eu_4Ga_{16}Ge_{30}$, *i.e.*, clathrates, with k_L = 0.6 W m^{-1} K^{-1}.[19]

b. Phonon group velocity, ν

The slope in the dispersion relation, $d\omega/dq_{ph}$, represents the phonon group velocity or propagation velocity of a wave packet, which is a very important quantity in heat transport. As shown in Fig. 2, the group velocity in the optical branch is almost negligible, resulting in insignificant heat conduction. In the acoustic branch, however, the group velocity is large in the long-wavelength (small-wavevector) regime but almost negligible at short wavelengths (near the edge of the Brillouin zone). Thus, the acoustic branch is responsible for thermal transport due to its large group velocity. At the long wavelength limit or continuum limit, the group velocity reaches the speed of sound in a crystal, c_s, which is related to elastic stiffness (related to chemical bonding), E, and mass density (related to the mass of the constituent atoms), ρ.

$$\lim_{q_{ph}\to 0} \nu = \lim_{q_{ph}\to 0} \frac{d\omega}{dq_{ph}} = c_s = \sqrt{\frac{E}{\rho}} \quad (3)$$

Therefore, a large atomic mass and weak chemical bonds result in low speeds of sound; the thermal conductivity can be reduced

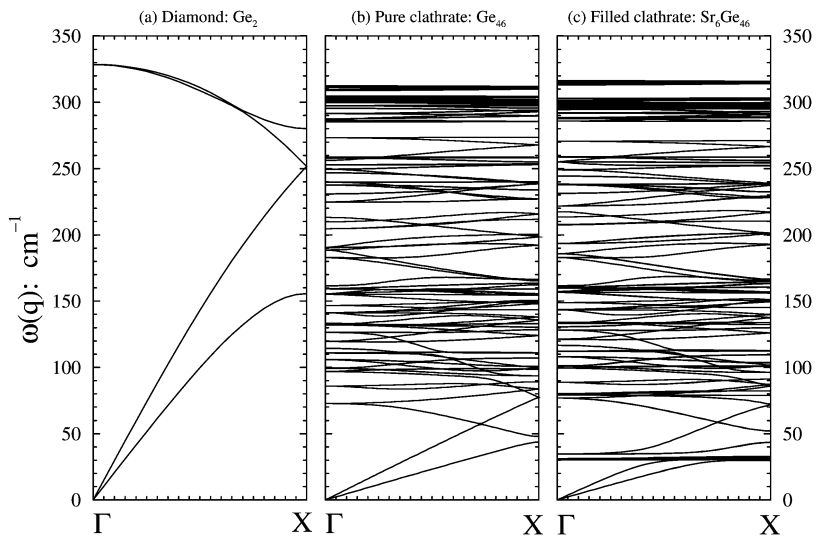

Fig. 2 The phonon dispersion curves of (a) diamond-structured Ge, (b) guest-free Ge_{46}, and (c) guest-containing clathrate Sr_6Ge_{46}.[15] LA, TA, LO, and TO denote the longitudinal acoustic, transverse acoustic, longitudinal optical, and transverse optical branches, respectively. Copyright © 2001, American Physical Society.

by choosing materials composed of heavy atoms and/or materials with weak bonding, like polymers.

Manipulating phonon group velocity is a very difficult problem due to the need to control the phonon dispersion relationship. Generally, phonon dispersion cannot be changed unless the feature size or characteristic length of the material is less than the phonon coherence length,[14,20] which is a few nanometers at most. Wingert *et al.*[21] reported sub-amorphous thermal conductivity in ~5 nm-thick crystalline Si nanotubes. They found that the reduced thermal conductivity could not be explained by boundary scattering alone, *i.e.*, Casimir limit, and claimed that changes in phonon dispersion or phonon group velocity were likely involved. A six-fold reduction in Young's modulus, *i.e.*, elastic stiffness, E, of the Si nanotubes compared to bulk Si was presented as a basis for the argument.

Simkin and Mahan[22] theoretically predicted a crossover between particle transport for thick layers to wave transport for thin layers in a multilayer structure, *e.g.*, superlattices. When the layer thickness decreases, interface scattering, *i.e.*, particle transport, increases and thermal conductivity decreases. However, when the layer thickness is small enough to affect phonon dispersion, wave interference effects, *i.e.*, wave transport, should occur. In this case, bandgaps appear in the phonon dispersion, resulting in an increase in thermal conductivity as the layer thickness decreases. As a result, the thermal conductivity is minimized at a certain period thickness. Fig. 3 shows the thermal conductivity of the $(SrTiO_3)_m/(CaTiO_3)_n$ superlattice *versus* period thickness, illustrating the existence of the minimum thermal conductivity.[23] The figure also presents a phonon dispersion curve showing the phonon bandgaps. Due to the standing wave generated by the constructive interference from Bragg reflection, the phonon group velocity is zero in the bandgaps, which reduces the thermal conductivity. However, in this case, it might be premature to conclude wave effects for short periods due to phonon bandgaps or whether there were simply poor interfaces due to inter-diffusion processes. To resolve this issue, a transmission electron micrograph (TEM) of a thin period showing the interface quality was also presented. Also, the thermal conductivity *versus* temperature measurement could help to further clarify the effects of phonon bandgaps on thermal conductivity. By varying the temperature, the dominant wavelength of a phonon can be changed due to Wien's displacement law for phonons.[24] Since phonon bandgap formation is related to the wavelength of the phonon and the period thickness of the superlattice, it should be possible to determine the location of the minimum in the thermal conductivity *versus* period thickness plot shift with temperature, which was demonstrated by Ravichandran *et al.*[23] in their study on the thermal conductivity of the $(SrTiO_3)_m/(CaTiO_3)_n$ superlattice.

c. Phonon mean free path, l

There are generally three types of phonon scattering: boundary, impurity and phonon–phonon interactions. The effective mean free path, l_{eff}, is expressed based on Matthiessen's rule[13,14] as below

$$\frac{1}{l_{eff}} = \frac{1}{l_b} + \frac{1}{l_i} + \frac{1}{l_{ph}}, \quad (4)$$

where l_b, l_i, and l_{ph} are the mean free path due to the boundary, impurity, and phonon–phonon scattering processes, respectively. There are two types of phonon–phonon scattering. One is called a normal process (N process), and the other is an Umklapp process (U process). Basically, eqn (4) indicates that the shortest mean free path dominates other scattering processes. To understand phonon scattering, the definition of a phonon is needed. A phonon is defined as the quantized energy of lattice vibration.[12,25] Lattice vibrations are based on a spring and mass system, so phonons get scattered whenever there is a difference in mass and/or spring constant. For example, an impurity for which the mass

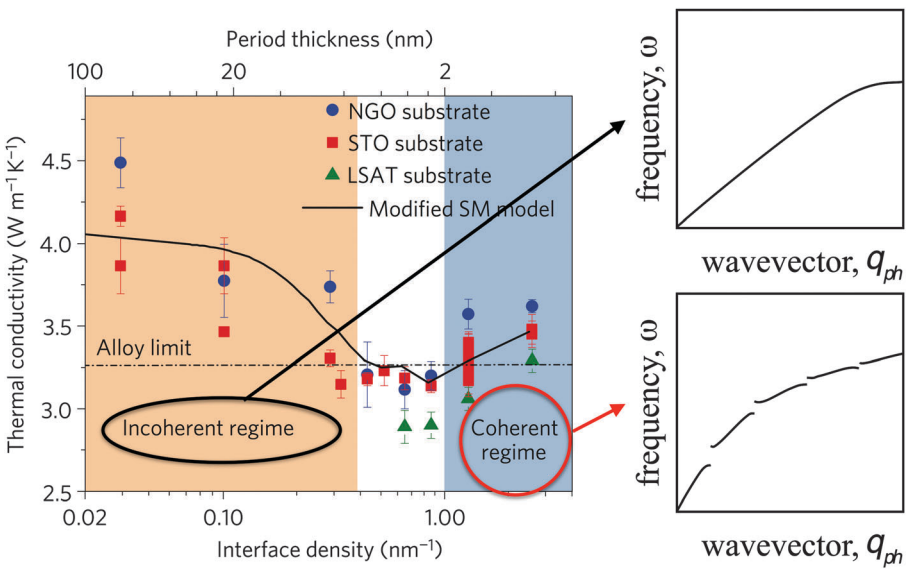

Fig. 3 Thermal conductivity of the $(SrTiO_3)_m/(CaTiO_3)_n$ superlattice *versus* period thickness.[23] A TEM figure shows the interface quality of the superlattice. Also, a phonon dispersion curve showing phonon bandgaps is presented.

and/or spring constant change with respect to its host medium can result in phonon scattering. This is called impurity scattering, which is elastic in nature (the energy of the incident phonon does not change). Another example of phonon scattering is phonon–phonon scattering, which is inelastic. This occurs even in pure crystals because of anharmonicity in the chemical bonds – a phonon is scattered due to changes in the spring constant upon stretching.

Measuring thermal conductivity *versus* temperature provides information regarding the dominant phonon scattering process. Fig. 4 shows the thermal conductivity of bulk silicon *versus* temperature,[26,27] where three different regimes indicate the dominant scattering process. The dependence of the scattering process on temperature can be explained by the spectral distribution of phonons and Wien's displacement law for phonons.[13] The phonon spectral distribution is almost the same as the blackbody distribution of photons. As in blackbody photon distribution, Wien's displacement law for phonons states that the wavelength of dominant heat carrying a phonon decreases as the temperature increases, *i.e.,* $\lambda_{max}T$ is constant. According to this law, long-wavelength phonons hold the most heat at low temperatures. A long-wavelength phonon is not impacted by defects, dislocations, *etc.*, which are on the atomic scale, because of the Rayleigh scattering criterion.[28,29] Such a phonon is mostly impacted by the boundary of the crystal. Therefore, at low temperatures, boundary scattering is dominant. As the temperature increases, the wavelength of dominant heat carrying phonons decreases. Hence, phonons will be scattered by defects, dislocations, *etc.* Impurity scattering is usually the dominant scattering process near the peak of thermal conductivity. At high temperatures, Umklapp or phonon-phonon scattering dominates over other scattering processes.

One issue in the temperature-dependent scattering process is the reference temperature. For example, a low temperature is low compared to the reference temperature. The Debye temperature, which is the temperature at which all phonon modes are excited,[12,25] serves as the reference temperature. The Debye temperature of silicon is 640 K.[30]

Fig. 4 shows the general trends for thermal conductivity *versus* temperature. In the region in which the temperature is much lower than the Debye temperature, boundary scattering dominates over other scattering processes. In the figure, the thermal conductivity increases with temperature, since the specific heat increases with temperature at low temperatures. The phonon group velocity can be approximated as the sound velocity, which is constant at low temperatures. The phonon mean free path is limited by the crystal boundary, which is also constant. Therefore, the only temperature dependency is that of the specific heat, which varies as the Debye's T^3 law.[13,14]

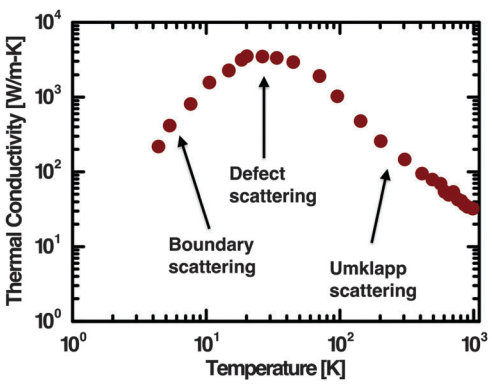

Fig. 4 Thermal conductivity of bulk silicon *versus* temperature.[26]

In the region where impurity scattering dominates over other scattering processes, the thermal conductivity reaches its peak. This usually occurs at approximately 1/10 of the Debye temperature.[13,14] Impurity scattering is highly frequency dependent, although it does not directly depend on temperature. On the other hand, the N process, which is temperature dependent, is closely related to impurity scattering because the N process redistributes phonon frequencies.[31] Therefore, the N process also plays an important role in determining the peak of thermal conductivity, where impurity scattering is important.

The only way thermal conductivity decreases with respect to temperature is the Umklapp process. For temperatures that are close to or higher than the Debye temperature, the number of phonons is proportional to temperature. Since the Umklapp process depends on the number of phonons, it becomes more dominant as the temperature is increased, and the phonon mean free path is inversely proportional to temperature, $\sim 1/T$. The specific heat has weak temperature dependence at high temperatures, and the temperature dependence of the phonon group velocity is not pronounced at high temperatures. Therefore, the temperature dependence of thermal conductivity at high temperatures mostly depends on that of the phonon mean free path. Thus, thermal conductivity is usually inversely proportional to temperature, $\sim 1/T$.

Grain boundary scattering, l_b. As the name indicates, boundary scattering is defined as phonon scattering due to a crystal boundary. This process is usually dominant for long-wavelength phonons and at low temperatures. Since most thermoelectric materials operate at room temperature or above, boundary scattering due to grains could be of practical importance. Therefore, we limit our discussion to grain boundary scattering, *i.e.*, grain boundary engineering. Grain boundary scattering can be combined with other scattering processes such as the all-scale hierarchical architecture,[10] where grain boundary scattering, alloy scattering, and nanoparticle scattering coexist in a material. In this review, however, we only discuss categorized strategies since a detailed review on the combined approaches can be found in the literature.[32,33] The schematic illustrations on the top part of Fig. 5 show the categories of grain boundary engineering that are either proposed or actively being researched: rough-surfaced grains, nano-sized grains, and coated grains.

The effective phonon mean free path of Si at room temperature is known to be around 300 nm.[34] If the crystal or grain boundary of Si is less than 300 nm at room temperature, the phonon mean free path decreases so the thermal conductivity is also reduced, as shown in Fig. 5(a), where the thermal conductivities of Si nanowires with different diameters are presented.[35,36] Li *et al.*[36]

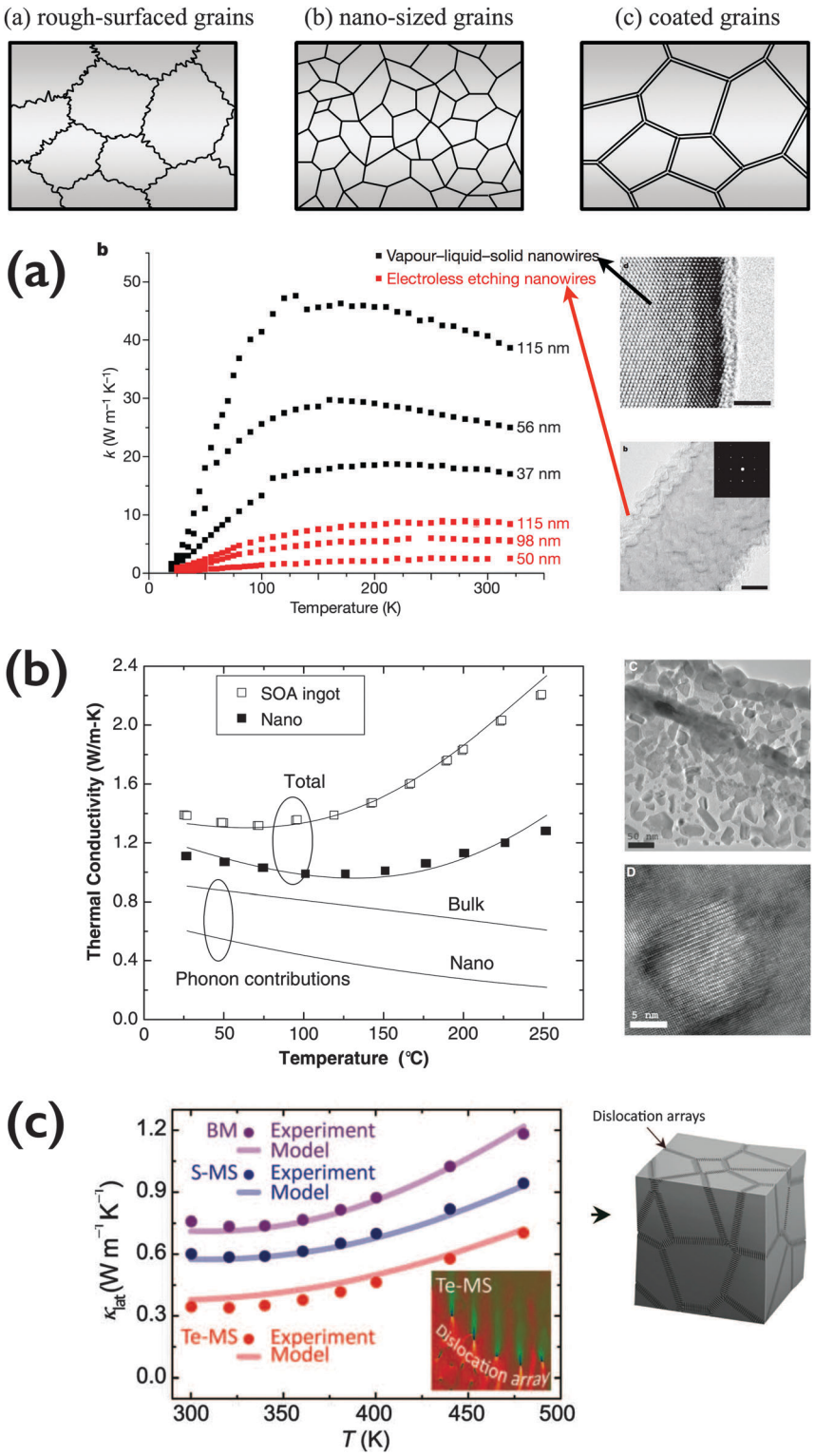

Fig. 5 Grain boundary engineering: (a) rough-surfaced grains, thermal conductivity of smooth (black dots) and rough (red dots) Si nanowires and TEM images of the nanowires.[35,36] Copyright © 2008, Rights Managed by Nature Publishing Group. Copyright © 2003 AIP Publishing LLC. (b) Nano-sized grains, thermal conductivity of a nanograined nanocomposite of BiSbTe.[81] Reprinted with permission from ref. 81 Copyright 2008 American Association for the Advancement of Science. (c) Coated grains, phonon thermal conductivity of $Bi_{0.5}Sb_{1.5}Te_{3.0}$ alloys produced by melt-solidification (ingot), solid-phase compaction (BM and S – MS), and liquid-phase compaction, *i.e.*, coated grains, (Te – MS).[47] Reprinted with permission from ref. 47 Copyright 2015 American Association for the Advancement of Science.

demonstrated that the thermal conductivity can be reduced from around 40 W m^{-1} K^{-1} to 18 W m^{-1} K^{-1} as the diameters decrease from 115 nm to 37 nm, as also shown in the figure. Considering that the thermal conductivity of bulk Si at room temperature is 140 W m^{-1} K^{-1},[26] this is quite a significant reduction. Hochbaum *et al.*[35] found that the thermal conductivities of rough Si nanowires (red dots in Fig. 5(a)) are significantly lower than those of smooth nanowires (black dots) even for those with the same diameter, *i.e.*, 115 nm. The reduction in thermal conductivity was too large to be explained with the Casimir limit. Although the exact reason for such a reduction is still in discussion, Kim *et al.*[37] proposed that the rough surface could at least scatter mid-frequency phonons. They found that the thermal conductivity of a rough $Si_{0.96}Ge_{0.04}$ nanowire is an order of magnitude lower than that of bulk $Si_{0.96}Ge_{0.04}$ and around a factor of four times lower than that of smooth $Si_{0.96}Ge_{0.04}$ nanowire. This significant reduction could be explained by the surface roughness scattering medium-wavelength phonons,[38] whereas the long-wavelength phonons are scattered by phonon boundary scattering, and the short-wavelength phonons are scattered by alloy scattering. In addition to the theoretical analysis, later experimental studies confirmed that the thermal conductivity of a rough nanowire is indeed lower than that of a smooth nanowire.[37,39–42] Therefore, it would be worthwhile to test the rough-surfaced grains to see if the thermal conductivity would be significantly reduced.

Fig. 5(b) shows the thermal conductivity of a nanograined nanocomposite. As shown in the SEM and TEM pictures, the nanocomposites are composed of nano-sized grains. Owing to the grain boundary scattering, the thermal conductivity of nanograined BiSbTe is lower than that of its bulk counterpart. This nanograined nanocomposite approach has been used with other materials[43–45] and is a well-established technique. Also, the interfacial states formed in the nanograined region can be used to increase the power factor, as proposed by Kirievsky *et al.*[46]

An example study of the coated-grain boundary is shown in Fig. 5(c). Kim *et al.*[47] synthesized Te-coated grains of $Bi_{0.5}Sb_{1.5}Te_{3.0}$ using the liquid-phase compaction strategy (Te – MS in Fig. 5(c)). They argued that the lower thermal conductivity of the coated grain composite than that of bulk $Bi_{0.5}Sb_{1.5}Te_{3.0}$ suggests that mid wavelength phonons are scattered by the coated grains; long- and short-wavelength phonons were scattered due to the grains and the alloy atoms, respectively, in the bulk $Bi_{0.5}Sb_{1.5}Te_{3.0}$, so only mid wavelength phonons possess thermal energy. While this argument seems reasonable, the model they used should be updated; the original model by Klemens[48] is for dislocation lines, *i.e.*, coated lines, which are oriented randomly, whereas the coated grains only occurred on the grain boundary. The model proposed by Chen *et al.*,[38] where interference effects in the coated grains due to Bragg reflection destroy the mid-wavelength phonons, might better describe this case. In any case, this work showed that the coated grains approach has superior potential for phonon engineering. There are also other good examples of coated grains in the literature.[49–52]

Impurity scattering, l_i. Phonons can be regarded as pseudo-particles. In this sense, kinetic theory can be used to explain phonon impurity scattering. According to kinetic theory, the mean free path due to an impurity is

$$l_i = \frac{1}{\sigma_{sct}(\chi) \cdot \eta} \quad (5)$$

where η denotes the impurity concentration, and σ_{sct} is the scattering cross-section, which is a function of χ, the size parameter. The size parameter is defined as the wavevector, q, of an incoming phonon multiplied by the radius of the scatter, R, *i.e.*, $\chi = qR$. The important parameter in impurity scattering is the scattering cross-section. When the size parameter approaches zero, the scattering cross-section forms according to the Rayleigh law. In the Rayleigh scattering regime, the scattering cross-section varies as $\sigma \sim d^6\omega^4$, where d is the size of the scattering particle, and ω is the phonon frequency. For atomic substitutions in alloys, $d \sim 1$ angstrom. The above relation suggests that short wavelength or Brillouin zone edge phonons are scattered much more effectively than mid- and long-wavelength phonons. At the other limit, where the size parameter approaches infinity, the scattering cross-section is independent of frequency.

In bulk materials, impurities are usually defects, vacancies, dislocations, *etc.*, which are on the order of the atomistic scale. Therefore, in bulk materials, the scattering cross-section follows the Rayleigh law, *i.e.*, $l \sim \omega^{-4}$. Fig. 6(a) shows the variation in phonon thermal conductivity with composition in the InAs–GaAs system.[53] This is a representative plot of the thermal conductivity of alloy materials; even with a small percentage of alloy atoms, the thermal conductivity can be dramatically reduced with maintained crystallinity of the material for efficient electrical transport. This is due to the short-wavelength phonons scattered by the alloy atoms or vacancies, *i.e.*, the Rayleigh law. At this time, the most efficient thermoelectric materials are alloys.

Although short-wavelength phonons can be scattered through alloy atoms or vacancies, long- to mid-wavelength phonons are not affected by alloy scattering and still possess thermal energy. Therefore, nanoparticles in alloy materials have been proposed to further scatter mid- to long-wavelength phonons, as shown in Fig. 6(b).[54,55] The figure shows the thermal conductivity of randomly distributed ErAs nanoparticles in $In_{0.53}Ga_{0.47}As$.[55] The thermal conductivity of ErAs in $In_{0.53}Ga_{0.47}As$ is lower than that of $In_{0.53}Ga_{0.47}As$ due to the scattering of mid-wavelenth phonons by the nanoparticles, as shown in the inset and schematic.[29] According to the analytical scattering cross-section of spherical nanoparticles as proposed by Kim and Majumdar,[29] it has been confirmed that nanoparticles do scatter mid- to long-wavelength phonons. Although the scattering cross-section for non-spherical particles should be developed since some of the nanostructures are not spherically shaped,[56] this analysis can serve as a good estimate. It is also well known that nanostructures significantly reduce thermal conductivity.[10,57,58] However, not all nanostructures reduce thermal conductivity; only some sizes of nanostructures decrease thermal conductivity.[6] Mingo *et al.*[59] performed an analysis regarding the optimal size of nanoparticles. Also, it is known that nanoparticles can be used to enhance the power

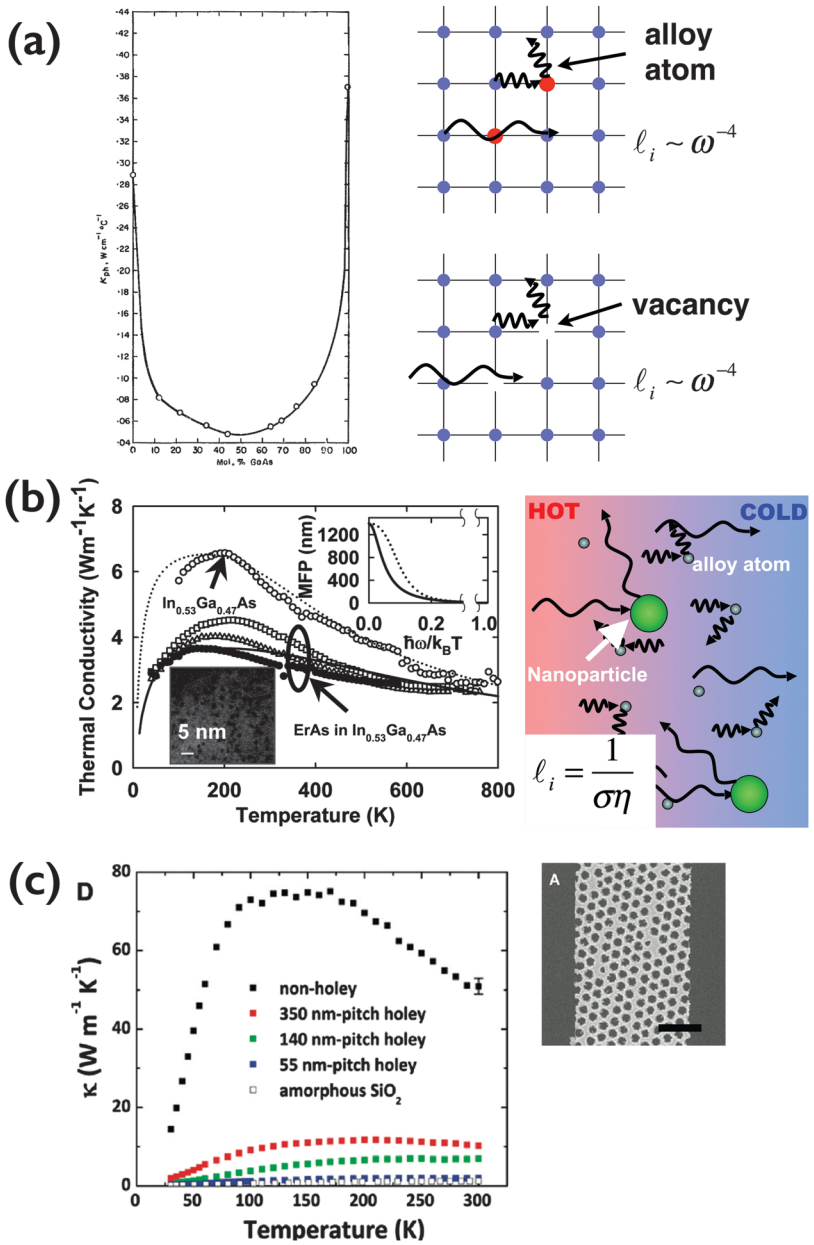

Fig. 6 (a) Variation of phonon thermal conductivity with the composition of the InAs–GaAs system.[53] Copyright managed by AIP Publishing LLC. The phonon mean free path in this case, *i.e.*, alloy scattering, depends on the frequency as $l \sim \omega^{-4}$ for either the alloy atom or the vacancy. (b) Thermal conductivity of randomly distributed ErAs nanoparticles in $In_{0.53}Ga_{0.47}As$.[55] The thermal conductivity of ErAs in $In_{0.53}Ga_{0.47}As$ is lower than that of $In_{0.53}Ga_{0.47}As$ due to the scattering of mid-wavelenth phonons by the nanoparticles shown in the inset and schematic.[29] Part (b) reprinted with permission from.[55] © 2006 American Institute of Physics. (c) Thermal conductivity of holey silicon as a function of temperature.[61] Diameters of the holes are from around 30 nm to 200 nm. Copyright © 2010, American Chemical Society.

factor due to the electron filtering effect; detailed analysis of this phenomenon is provided by Faleev *et al.*[60]

Fig. 6(c) shows the thermal conductivity of holey silicon as a function of temperature.[61] The diameters of the holes range from around 30 nm to 200 nm. Changes in phonon dispersion can be ruled out since the smallest size of the silicon is larger than 20 nm; it is known that changes in phonon dispersion do not occur unless the feature size is less than ~20 nm.[62,63] It was expected that the holes functioned to scatter phonons in the same way, with either the alloy atom or vacancy treated as a point defect.[48] In this case, we regard the hole as a nano-sized impurity without mass, which then serves as a very strong scatter source since, according to theory,[29,48,64] the scattering strength is proportional to $[(M_h - M_i)/M_h]^2 \sim (\Delta M/M_h)^2$, where M_h and M_i are masses of the host and impurity, respectively. Although ΔM is typically less than unity, it is unity in the case of a hole. Therefore, one can expect strong scattering in the presence of nano-sized holes. However, care should be taken

when using the scattering cross-section of nanoparticles to analyze scattering due to nano-sized holes since the analysis for spherical nanoparticles is based on the perturbation method,[29] where differences in mass between the host and nanoparticles are small. However, Cahill *et al.*[65] suggested that the pertubation analysis is still valid even when the mass contrast is larger than unity in point defect scattering. A comparison of the experimental data and theoretical analysis for nano-sized holes is needed to clarify this point. Similarly, Yu *et al.*[66] demonstrated that the thermal conductivity of Si can be reduced significantly by patterning the Si onto nano-sized mesh structures. In this case, some of the feature sizes are less than 20 nm, so changes in the phonon dispersion are possible.[62,63]

Phonon–phonon scattering, l_{ph}. Phonon–phonon scattering is a consequence of anharmonicity of the chemical bond. So far, our discussion has basically assumed that the inter-atomic interaction is harmonic. In other words, the spring constant does not change despite the large deviation of the atom from its equilibrium position. This is not true in an actual crystal. For large atomic displacements from their lattice positions, the force constant (spring constant) is not the same as that under a harmonic approximation. Since phonons involve atomic displacements, the lattice is distorted, and the spring constant is changed as it travels. When a second phonon is incident on the same region, it is scattered because of changes in the spring constant.

Both impurity scattering and phonon–phonon scattering determine the mean free path of phonons. However, the mean free path alone cannot determine the thermal conductivity. Thermal conductivity inherently assumes local thermodynamic equilibrium, in which phonon–phonon scattering plays an important role because of the inelastic nature of phonon–phonon scattering.

Phonon–phonon scattering is an intrinsic process, so externally increasing the scattering rate is quite difficult. For this reason, methods to change the scattering rate have not been explored as much as those of the boundary and impurity scattering rates. In this review, we present two methods as examples, *i.e.*, lone-pair electrons and acoustical-to-optical phonon scattering.

At high temperatures, when only acoustic phonons participate in the thermal transport and the Umklapp scattering process dominates other processes, the phonon thermal conductivity can be written as[67–69]

$$k_L \approx A\frac{M_a\theta^3\delta}{\gamma^2 n^{2/3}T} \quad (6)$$

where A is a constant, M_a is the average mass of the atoms in a crystal, θ is the Debye temperature, δ^3 is the volume per atom, n is the number of atoms in the primitive unit cell, and γ is the Grüneisen parameter. The Grüneisen parameter is deduced from Grüneisen's law of thermal expansion[64] and is a direct measure of anharmonicity of bonds.[68] The parameter quantifies the effect of changes in interatomic distance on bond stiffness.[70] As shown in eqn (6), the higher is the Grüneisen parameter, *i.e.*, higher anharmonicity, the lower is the phonon thermal conductivity.

Skoug and Morelli[71] proposed that lone-pair electrons can reduce phonon thermal conductivity in some chalcogenide compounds. As shown in the schematics of Cu_3SbSe_3 and $CuSbSe_2$ in Fig. 7(a), the electrostatic repulsion between lone-pair electrons and neighboring chalcogen ions creates anharmonicity, increasing the Grüneisen parameter. This concept has been further validated by Nielsen *et al.*,[70] who showed that the thermal conductivity of $AgSbSe_2$ could be reduced to the amorphous limit. The Grüneisen parameter of $AgSbSe_2$ is as large as $\gamma = 3.7$,[70] compared to the $\gamma \sim 1.4$[68] of PbTe.

Another way of reducing the phonon thermal conductivity through phonon–phonon scattering is 'acoustical to optical phonon scattering,' as explained below. An important relationship that can be deduced from the dispersion relation is that the frequency gap between the acoustic and the optical branches is closely related to the atomic mass ratio of the constituent atoms in the unit cell.[12,13,72] The frequency gap becomes smaller when the mass ratio approaches unity, as shown in Fig. 7(b). Vibrations of the crystal within a frequency in the gap cannot propagate in the crystal and are extinguished. Steigmeier and Kudman[72] proposed that this frequency gap between the acoustical and optical branches is related to phonon thermal conductivity since the size of the gap determines the Umklapp scattering rate. As shown in Fig. 7(b), when the gap is small, the probability of a low-frequency phonon, *i.e.*, a long-wavelength phonon, participating in the Umklapp scattering process is high. This means that a low-frequency phonon, which has a higher group velocity than the high-frequency phonon, can be scattered into the optical phonon,

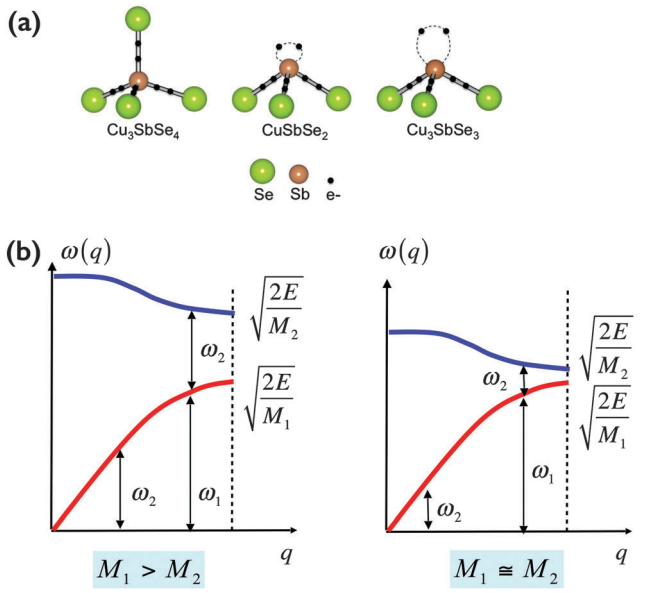

Fig. 7 (a) Schematic representation of the lone-pair electron with illustration of the local atomic enviroment of Sb in Cu_3SbSe_4, Cu_3SbSe_3, and $CuSbSe_2$.[71] Dashed lines indicate the approximate morphology of the Sb lone-pair 5s electron orbital. Copyright © 2011 American Physical Society. (b) Schematic showing the acoustical-to-optical phonon scattering process. The mass ratio of constituent atoms is related to the gap between the acoustical and optical branches.

which has a negligible impact on the thermal transport due to its near zero group velocity. Therefore, by choosing the mass ratio of the constituent atoms, acoustical phonons can be scattered into optical phonons, thereby reducing the thermal conductivity. In a similar way, Delaire *et al.*[73] suggested that strong anharmonic coupling between longitudinal acoustic (LA) and transverse optical (TO) modes could be the reason for the low thermal conductivity in PbTe. Using the phonon dispersion relationship measured by neutron scattering along with first-principles computations, they claimed that there should exist LA + TO − LO scattering processes, which significantly reduce thermal conductivity.

3. Comments on the Wiedemann–Franz law

The electronic thermal conductivity is usually estimated using the Wiedemann–Franz law,[14,25] which is expressed as below

$$k_e = \sigma L T, \tag{7}$$

where the Lorenz number, L, for a semiconductor (equation 4.1.19 in ref. 74) is

$$L = \frac{{k_B}^2}{e^2}\left[\frac{\left(p+\frac{7}{2}\right)\left(p+\frac{3}{2}\right)F_{\left(p+\frac{5}{2}\right)}F_{\left(p+\frac{1}{2}\right)} - \left(p+\frac{5}{2}\right)^2 F_{\left(p+\frac{3}{2}\right)}{}^2}{\left(p+\frac{3}{2}\right)^2 F_{\left(p+\frac{1}{2}\right)}{}^2}\right], \tag{8}$$

where e is the electronic charge, and k_B is the Boltzmann constant. Here, p appears when estimating the relaxation time, τ, as

$$\tau \approx E^p, \tag{9}$$

where E is the energy of electrons. F in eqn (8) is the Fermi–Dirac integral of order r, which is

$$F_r(\eta_F) = \int_0^\infty \frac{x^r}{1+e^{x-\eta_F}}\mathrm{d}x, \tag{10}$$

where η_F is the reduced Fermi energy. For example, in an n-type semiconductor, η can be written as

$$\eta_F = \frac{E_F - E_C}{k_B T}, \tag{11}$$

where E_F and E_C are the energy of the Fermi level and the conduction band, respectively. Eqn (8) reveals that the Lorenz number for a semiconductor is a function of the position of the Fermi level and the relaxation time of the electrons. The Lorenz number in the non-degenerate regime is $2(k_B/e)^2$ or $4(k_B/e)^2$, while that in the degenerate regime is $(\pi^2/3) \times (k_B/e)^2$, which is the same as the Lorenz number for metal.

However, the Wiedemann Franz law is only valid when the momentum relaxation time governing the electrical conductivity is the same as the energy relaxation time governing the electronic thermal conductivity.[25] This validity breaks down when the temperature approaches the Debye temperature.[75] In this case, the electronic thermal conductivity tends to be less than that predicted by the Wiedemann–Franz law. For example, the experimentally determined Lorenz number of InSb is only 60 percent of the Lorenz number predicted by the Wiedemann–Franz law near the Debye temperature.[76] According to Ziman,[64] the explanation is as follows. When electron–phonon scattering occurs, the momentum and energy conservation are

$$\begin{aligned} \hbar\vec{q}_{e,\mathrm{incoming}} + \hbar\vec{q}_{ph} &= \hbar\vec{q}_{e,\mathrm{scattered}} \\ \frac{\hbar^2\left|\vec{q}_{e,\mathrm{incoming}}\right|^2}{2m^*} + \hbar\omega &= \frac{\hbar^2\left|\vec{q}_{e,\mathrm{scattered}}\right|^2}{2m^*} \end{aligned} \tag{12}$$

where q_e is the wavevector of an electron, and q_{ph} is the wavevector of a phonon. Below the Debye temperature, the change in the electron propagation direction is small ("small angle scattering"), as shown in Fig. 8(a). This is because the magnitude of the phonon wavevector is small below the Debye temperature, so the electron needs to scatter multiple times to relax the momentum. However, according to Wien's displacement law for phonons,[13] the energy of a phonon, $\hbar\omega$, is proportional to k_BT below the Debye temperature. Thus, the phonon energy in this temperature range is sufficient to change a 'hot' electron to 'cold,' and *vice versa*, as shown in Fig. 8(b), where f_0 denotes the Fermi–Dirac distribution. An electron can be categorized as hot or cold depending on whether the energy of the electron is higher or lower than the Fermi energy. Even though the temperature is slightly higher than the Debye temperature, scattering through a large angle merely turns a hot electron traveling east into a cold electron traveling west and thus has little effect on the electrical current.[64] Therefore, electron-phonon scattering is a very efficient mechanism for electron energy relaxation but not for electron momentum relaxation. As a result of these arguments, the momentum relaxation time is larger than the energy relaxation time of an electron near the Debye temperature, *i.e.*, the Lorenz number decreases.

The Wiedemann–Franz law is valid when the temperature is either significantly lower or higher than the Debye temperature. At low temperature, the dominant scattering mechanism for an electron is impurity scattering, which is elastic in nature. In this case, the momentum relaxation time is approximately the

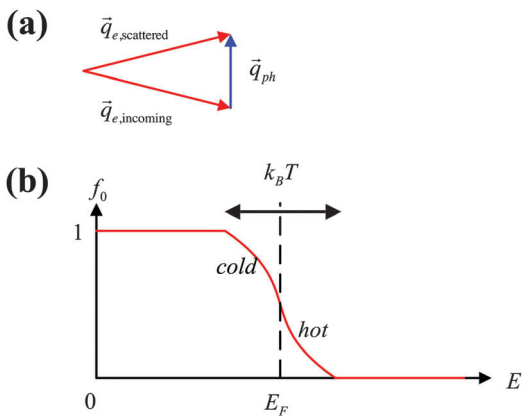

Fig. 8 (a) Small angle scattering of electrons near the Debye temperature. (b) Fermi–Dirac distribution of electrons.

same as the energy relaxation time. At high temperature, the maximum amount of energy gained or lost by an electron during the electron–phonon scattering process is limited to $k_B\theta_D$, where θ_D is the Debye temperature.[64] Only when $k_BT \gg k_B\theta_D$, electron–phonon scattering ceases to be an efficient mechanism for electron energy relaxation. This electron–phonon scattering is regarded as 'quasi-elastic scattering' because $k_BT \gg k_B\theta_D$ at high temperature. Therefore, another way of stating the validity of this law is that it is valid as long as the scattering is elastic.[64]

One more thing to note is that the Wiedemann–Franz law does not consider the bipolar thermal conductivity.[77] For this reason, when Lukas *et al.*[78] experimentally determined the Lorenz number of $Bi_{0.88}Sb_{0.12}$, they measured up to temperatures around 140 K, whereas the onset of the bipolar thermal conductivity effect occurred at temperatures higher than 150 K. Below 140 K, they found that those are matched with eqn (8). In this case, the Debye temperature of $Bi_{0.88}Sb_{0.12}$ should lie somewhere between the Debye temperature of Bi, *i.e.*, 112 K, and that of Sb, *i.e.*, 204 K.[79] Also, Kim *et al.*[77] proposed an updated model to compensate for this discrepancy of the Wiedemann–Franz law.

4. Summary and outlook

In this review, we discussed some of the representative strategies for phonon engineering by categorizing them into methods affecting each component of phonon thermal conductivity, *i.e.*, specific heat, phonon group velocity, and mean free path. We further categorized the mean free path, *i.e.*, scattering processes, into grain boundary scattering, impurity scattering, and phonon–phonon scattering. The brief summary is as follows.

A large unit cell approach was suggested for reducing the specific heat by utilizing the nearly zero phonon group velocity of the optical branch. When the number of atoms increases in a unit cell, this induces an increase in optical branch since the total number of acoustic branches is limited to 3; 1 in longitudinal and 2 in transverse acoustic branches. Therefore, the material absorbs heat, but only a small fraction of the energy is transported through the acoustic branch. Note that the phonon group velocity in the acoustic branches also decreases in this case since the maximum phonon frequency is limited to around 10 THz and the ranges of the optical branches increase.

The phonon group velocity is a slope in the phonon dispersion relationship. In the long wavelength limit, the phonon group velocity approaches the speed of sound. To reduce the speed of sound, weak bonding and heavy mass are required. It is challenging to change the phonon dispersion since a feature size of a material should be less than the phonon coherence length in a rough estimation. However, this can be implemented in the superlattice structure. Due to the standing wave generated owing to the constructive interference by Bragg reflection, phonon bandgaps can be generated within the acoustic branch, which reduces the thermal conductivity because the phonon group velocity becomes zero at the bandgap. Although there is some experimental data supporting this hypothesis, further verification is needed. A solution for bulk material should also be proposed in the future.

We discussed three types of grain boundaries: rough-surfaced grains, nano-sized grains, and coated grains. Although rough-surfaced grains have not yet been demonstrated, it is known that the thermal conductivity of rough-surfaced nanowires is significantly lower than the Casimir limit. Thus, if rough-surfaced grains were implemented, a significant reduction in thermal conductivity could be anticipated. Nano-sized grains are now a well-established technique. Nano-sized grains severely scatter phonons, which causes the thermal conductivity to decrease. Further study is needed to determine how to synthesize nano-sized grains in various and economically viable ways and how to inhibit grain growth. The idea of coated grains has been proposed, and there are experimental results to support this hypothesis. Although a theory to explain scattering due to coated grains should be developed, the experimental data for coated grains look very promising for thermoelectric applications.

We addressed four different types of impurity scattering: alloy atoms, vacancies, nanoparticles, and nano-sized holes. It is well known that alloying is a very efficient way to reduce thermal conductivity while maintaining the crystallinity of a material to ensure decent electrical transport. Scattering due to both alloy atoms and vacancies follows the Rayleigh law, which predicts selective scattering of short-wavelength phonons. To further reduce the thermal conductivity by scattering mid- to long-wavelength phonons, nanoparticles embedded epitaxially have been proposed, which is also a well-known concept. Experimental results show remarkable reductions in thermal conductivity of a material containing nano-sized holes. In such material, the feature size between holes is larger than the phonon coherence length, so changes in phonon dispersion might not occur. It is uncertain whether the scattering cross-section developed for nanoparticle scattering can be applied to nano-sized holes since the reduction seems rather dramatic. This also requires further study both in theory and experiment.

Unlike grain boundary and impurity scatterings, phonon–phonon scattering is inelastic and intrinsic. Therefore, it is not trivial to enhance the scattering rate through external means. We have provided two such ways. One is lone-pair electrons, and the other is acoustical-to-optical phonon scattering. The electrostatic repulsion between lone-pair electrons and neighboring chalcogen ions creates anharmonicity, increasing the Grüneisen parameter. Acoustical phonons can efficiently be promoted to optical phonons by phonon–phonon scattering in a material with a small gap between the acoustic and optical branches. This can occur when the mass difference of constituent atoms is small.

In addition, comments on the Wiedemann–Franz law were provided to emphasize the limitation of the law, and there exist temperature ranges where this law can serve as a good estimation of electronic thermal conductivity.

We should mention that the categorization of strategies for phonon engineering is not perfect since some of the strategies are cross-related with other strategies. We hope that

this categorization provides an organized view of phonon engineering such that this concept can be implemented synergistically with power factor enhancement approaches when material chemists or scientists design a thermoelectric material.

Acknowledgements

The author thanks Dr Pankaj Kumar Rawat, Chanyoung Kang, Jungwon Kim, and Hwanjoo Park for help with the figures and comments. This work was supported by the Mid-career Researcher Program (No. 2011-0028729) and the Nano-Material Technology Development Program (Green Nano Technology Development Program) (No. 2011-0030146) through a National Research Foundation of Korea (NRF) grant funded by the Ministry of Education, Science and Technology (MEST).

References

1 L. E. Bell, *Science*, 2008, **321**, 1457–1461.
2 A. Majumdar, *Science*, 2004, **303**, 777–778.
3 G. A. Slack, New Materials and Performance Limit for Thermoelectric Cooling, in *CRC Handbook of Thermoelectrics*, ed. D. M. Rowe, CRC Press, 1995.
4 D. M. Rowe, *CRC Handbook of Thermoelectrics: Macro to Nano*, CRC/Taylor and Francis, Boca Raton, FL, 2006.
5 http://voyager.jpl.nasa.gov/mission/index.html.
6 H. Wang, J.-H. Bahk, C. Kang, J. Hwang, K. Kim, J. Kim, P. Burke, J. E. Bowers, A. C. Gossard, A. Shakouri and W. Kim, *Proc. Natl. Acad. Sci. U. S. A.*, 2014, **111**, 10949–10954.
7 H. Wang, J. Hwang, M. L. Snedaker, I.-h. Kim, C. Kang, J. Kim, G. D. Stucky, J. Bowers and W. Kim, *Chem. Mater.*, 2015, **27**, 944–949.
8 H. J. Wu, L. D. Zhao, F. S. Zheng, D. Wu, Y. L. Pei, X. Tong, M. G. Kanatzidis and J. Q. He, *Nat. Commun.*, 2014, **5**, 4515.
9 L.-D. Zhao, S.-H. Lo, Y. Zhang, H. Sun, G. Tan, C. Uher, C. Wolverton, V. P. Dravid and M. G. Kanatzidis, *Nature*, 2014, **508**, 373–377.
10 K. Biswas, J. He, I. D. Blum, C.-I. Wu, T. P. Hogan, D. N. Seidman, V. P. Dravid and M. G. Kanatzidis, *Nature*, 2012, **489**, 414–418.
11 F. J. DiSalvo, *Science*, 1999, **285**, 703–706.
12 C. Kittel, *Introduction to solid state physics*, John Wiley & Sons, New York, 1996.
13 C. L. Tien, A. Majumdar and F. M. Gerner, *Microscale energy transport*, Taylor & Francis, Washington, D.C., 1998.
14 G. Chen, *Nanoscale energy transport and conversion*, Oxford University Press, New York, 2005.
15 J. J. Dong, O. F. Sankey and C. W. Myles, *Phys. Rev. Lett.*, 2001, **86**, 2361–2364.
16 B. Wölfing, C. Kloc, J. Teubner and E. Bucher, *Phys. Rev. Lett.*, 2001, **86**, 4350–4353.
17 D. M. Babanly, S. V. Askerova, M. B. Babanly and Y. A. Yusibov, *Russ. J. Inorg. Chem.*, 2011, **56**, 1114–1118.
18 J. Teubner, *Optimization of high efficiency thermoelectrics based on Tl5Te3*, PhD thesis, Department of Physics, University of Konstanz, 2001.
19 J. L. Cohn, G. S. Nolas, V. Fessatidis, T. H. Metcalf and G. A. Slack, *Phys. Rev. Lett.*, 1999, **82**, 779–782.
20 G. Chen, *Journal of Heat Transfer-Transactions of the ASME*, 1997, **119**, 220–229.
21 M. C. Wingert, S. Kwon, M. Hu, D. Poulikakos, J. Xiang and R. Chen, *Nano Lett.*, 2015, **15**, 2605–2611.
22 M. V. Simkin and G. D. Mahan, *Phys. Rev. Lett.*, 2000, **84**, 927–930.
23 J. Ravichandran, A. K. Yadav, R. Cheaito, P. B. Rossen, A. Soukiassian, S. J. Suresha, J. C. Duda, B. M. Foley, C.-H. Lee, Y. Zhu, A. W. Lichtenberger, J. E. Moore, D. A. Muller, D. G. Schlom, P. E. Hopkins, A. Majumdar, R. Ramesh and M. A. Zurbuchen, *Nat. Mater.*, 2014, **13**, 168–172.
24 A. Majumdar, *Journal of Heat Transfer-Transactions of The ASME*, 1993, **115**, 7–16.
25 N. W. Ashcroft and N. D. Mermin, *Solid state physics*, Holt Rinehart and Winston, New York, 1976.
26 C. J. Glassbrenner and G. A. Slack, *Phys. Rev.*, 1964, **134**, A1058–A1069.
27 S. T. Huxtable, *Heat transport in superlattices and nanowire arrays*, PhD thesis, Mechanical Engineering, University of California Berkeley, 2002.
28 B. Abeles, *Phys. Rev.*, 1963, **131**, 1906–1911.
29 W. Kim and A. Majumdar, *J. Appl. Phys.*, 2006, **99**, 084306.
30 http://www.ioffe.rssi.ru/SVA/NSM/Semicond/Si/basic.html.
31 J. Callaway, *Phys. Rev.*, 1959, **113**, 1046–1051.
32 N. A. Heinz, T. Ikeda, Y. Pei and G. J. Snyder, *Adv. Funct. Mater.*, 2014, **24**, 2135–2153.
33 D. L. Medlin and G. J. Snyder, *Curr. Opin. Colloid Interface Sci.*, 2009, **14**, 226–235.
34 Y. S. Ju and K. E. Goodson, *Appl. Phys. Lett.*, 1999, **74**, 3005–3007.
35 A. I. Hochbaum, R. Chen, R. D. Delgado, W. Liang, E. C. Garnett, M. Najarian, A. Majumdar and P. Yang, *Nature*, 2008, **451**, 163–167.
36 D. Y. Li, Y. Y. Wu, P. Kim, L. Shi, P. D. Yang and A. Majumdar, *Appl. Phys. Lett.*, 2003, **83**, 2934–2936.
37 H. Kim, Y. H. Park, I. Kim, J. Kim, H. J. Choi and W. Kim, *Appl. Phys. A: Mater. Sci. Process.*, 2011, **104**, 23–28.
38 R. Chen, A. I. Hochbaum, P. Murphy, J. Moore, P. D. Yang and A. Majumdar, *Phys. Rev. Lett.*, 2008, **101**, 105501.
39 J. P. Feser, J. S. Sadhu, B. P. Azeredo, K. H. Hsu, J. Ma, J. Kim, M. Seong, N. X. Fang, X. Li, P. M. Ferreira, S. Sinha and D. G. Cahill, *J. Appl. Phys.*, 2012, **112**, 114306.
40 K. Hippalgaonkar, B. L. Huang, R. K. Chen, K. Sawyer, P. Ercius and A. Majumdar, *Nano Lett.*, 2010, **10**, 4341–4348.
41 J. W. Lim, K. Hippalgaonkar, S. C. Andrews, A. Majumdar and P. D. Yang, *Nano Lett.*, 2012, **12**, 2475–2482.
42 Y. H. Park, J. Kim, H. J. Choi, H. Kim, I. Kim, K. Y. Lee, D. Seo and W. Kim, *Appl. Phys. A: Mater. Sci. Process.*, 2011, **104**, 7–14.
43 G. Joshi, H. Lee, Y. Lan, X. Wang, G. Zhu, D. Wang, R. W. Gould, D. C. Cuff, M. Y. Tang, M. S. Dresselhaus, G. Chen and Z. Ren, *Nano Lett.*, 2008, **8**, 4670–4674.

44 W. Xie, J. He, H. J. Kang, X. Tang, S. Zhu, M. Laver, S. Wang, J. R. D. Copley, C. M. Brown, Q. Zhang and T. M. Tritt, *Nano Lett.*, 2010, **10**, 3283–3289.
45 S. K. Bux, R. G. Blair, P. K. Gogna, H. Lee, G. Chen, M. S. Dresselhaus, R. B. Kaner and J.-P. Fleurial, *Adv. Funct. Mater.*, 2009, **19**, 2445–2452.
46 K. Kirievsky, M. Shlimovich, D. Fuks and Y. Gelbstein, *Phys. Chem. Chem. Phys.*, 2014, **16**, 20023–20029.
47 S. I. Kim, K. H. Lee, H. A. Mun, H. S. Kim, S. W. Hwang, J. W. Roh, D. J. Yang, W. H. Shin, X. S. Li, Y. H. Lee, G. J. Snyder and S. W. Kim, *Science*, 2015, **348**, 109–114.
48 P. G. Klemens, *Proc. Phys. Soc., London, Sect. A*, 1955, **68**, 1113.
49 B. Zhang, J. He, X. Ji, T. M. Tritt and A. Kumbhar, *Appl. Phys. Lett.*, 2006, **89**, 163114.
50 X. Ji, J. He, Z. Su, N. Gothard and T. M. Tritt, *J. Appl. Phys.*, 2008, **104**, 034907.
51 L. Fu, J. Yang, J. Peng, Q. Jiang, Y. Xiao, Y. Luo, D. Zhang, Z. Zhou, M. Zhang, Y. Cheng and F. Cheng, *J. Mater. Chem. A*, 2015, **3**, 1010–1016.
52 P. Puneet, R. Podila, S. Zhu, M. J. Skove, T. M. Tritt, J. He and A. M. Rao, *Adv. Mater.*, 2013, **25**, 1033–1037.
53 M. S. Abrahams, R. Braunstein and F. D. Rosi, *J. Phys. Chem. Solids*, 1959, **10**, 204–210.
54 W. Kim, S. L. Singer, A. Majumdar, J. M. O. Zide, D. Klenov, A. C. Gossard and S. Stemmer, *Nano Lett.*, 2008, **8**, 2097–2099.
55 W. Kim, J. Zide, A. Gossard, D. Klenov, S. Stemmer, A. Shakouri and A. Majumdar, *Phys. Rev. Lett.*, 2006, **96**, 045901.
56 J. He, J. Androulakis, M. G. Kanatzidis and V. P. Dravid, *Nano Lett.*, 2012, **12**, 343–347.
57 K. F. Hsu, S. Loo, F. Guo, W. Chen, J. S. Dyck, C. Uher, T. Hogan, E. K. Polychroniadis and M. G. Kanatzidis, *Science*, 2004, **303**, 818–821.
58 K. Biswas, J. Q. He, Q. C. Zhang, G. Y. Wang, C. Uher, V. P. Dravid and M. G. Kanatzidis, *Nat. Chem.*, 2011, **3**, 160–166.
59 N. Mingo, D. Hauser, N. P. Kobayashi, M. Plissonnier and A. Shakouri, *Nano Lett.*, 2009, **9**, 711–715.
60 S. V. Faleev and F. Léonard, *Phys. Rev. B: Condens. Matter Mater. Phys.*, 2008, **77**, 214304.
61 J. Tang, H.-T. Wang, D. H. Lee, M. Fardy, Z. Huo, T. P. Russell and P. Yang, *Nano Lett.*, 2010, **10**, 4279–4283.
62 D. G. Cahill, P. V. Braun, G. Chen, D. R. Clarke, S. Fan, K. E. Goodson, P. Keblinski, W. P. King, G. D. Mahan, A. Majumdar, H. J. Maris, S. R. Phillpot, E. Pop and L. Shi, *Appl. Phys. Rev.*, 2014, **1**, 011305.
63 N. Mingo, *Phys. Rev. B: Condens. Matter Mater. Phys.*, 2003, **68**, 113308.
64 J. Ziman, *Electrons and phonons*, Oxford University Press, Oxford, 2001.
65 D. G. Cahill, F. Watanabe, A. Rockett and C. B. Vining, *Phys. Rev. B: Condens. Matter Mater. Phys.*, 2005, **71**, 235202.
66 J.-K. Yu, S. Mitrovic, D. Tham, J. Varghese and J. R. Heath, *Nat. Nanotechnol.*, 2010, **5**, 718–721.
67 C. L. Julian, *Phys. Rev.*, 1965, **137**, A128–A137.
68 D. T. Morelli, V. Jovovic and J. P. Heremans, *Phys. Rev. Lett.*, 2008, **101**, 035901.
69 G. A. Slack, *J. Phys. Chem. Solids*, 1973, **34**, 321–335.
70 M. D. Nielsen, V. Ozolins and J. P. Heremans, *Energy Environ. Sci.*, 2013, **6**, 570–578.
71 E. J. Skoug and D. T. Morelli, *Phys. Rev. Lett.*, 2011, **107**, 235901.
72 E. F. Steigmeier and I. Kudman, *Phys. Rev.*, 1966, **141**, 767–774.
73 O. Delaire, J. Ma, K. Marty, A. F. May, M. A. McGuire, M. H. Du, D. J. Singh, A. Podlesnyak, G. Ehlers, M. D. Lumsden and B. C. Sales, *Nat. Mater.*, 2011, **10**, 614–619.
74 J. R. Drabble and H. J. Goldsmid, *Thermal conduction in semiconductors*, Pergamon Press, Oxford, New York, 1961.
75 G. S. Kumar, G. Prasad and R. O. Pohl, *J. Mater. Sci.*, 1993, **28**, 4261–4272.
76 M. A. Alieva, S. A. Aliev and M. I. Aliev, *Semiconductors*, 1970, **3**, 1331–1333.
77 H.-S. Kim, Z. M. Gibbs, Y. Tang, H. Wang and G. J. Snyder, *APL Mater.*, 2015, **3**, 041506.
78 K. C. Lukas, W. S. Liu, G. Joshi, M. Zebarjadi, M. S. Dresselhaus, Z. F. Ren, G. Chen and C. P. Opeil, *Phys. Rev. B: Condens. Matter Mater. Phys.*, 2012, **85**, 205410.
79 P. Fischer, I. Sosnowska and M. Szymanski, *J. Phys. C: Solid State Phys.*, 1978, **11**, 1043.
80 Q. Guo, M. Chan, B. A. Kuropatwa and H. Kleinke, *Chem. Mater.*, 2013, **25**, 4097–4104.
81 B. Poudel, Q. Hao, Y. Ma, Y. Lan, A. Minnich, B. Yu, X. Yan, D. Wang, A. Muto, D. Vashaee, X. Chen, J. Liu, M. S. Dresselhaus, G. Chen and Z. Ren, *Science*, 2008, **320**, 634–638.